



Quantitative evaluation of nanoparticle classification by size-exclusion chromatography

Sebastian Süß^{a,b}, Christoph Metzger^c, Cornelia Damm^{a,b}, Doris Segets^{a,b}, Wolfgang Peukert^{a,b,*}

^a Institute of Particle Technology (LFG), Friedrich-Alexander-Universität Erlangen-Nürnberg (FAU), Cauerstr. 4, 91058 Erlangen, Germany

^b Interdisciplinary Center for Functional Particle Systems (FPS), Friedrich-Alexander-Universität Erlangen-Nürnberg (FAU), Haberstraße 9a, 91058 Erlangen, Germany

^c Process Systems Engineering (SVT), Technische Universität München (TUM), Gregor-Mendel-Straße 4, 85354 Freising, Germany

ARTICLE INFO

Article history:

Received 21 February 2018

Received in revised form 31 July 2018

Accepted 2 August 2018

Available online 3 August 2018

Keywords:

Separation

Chromatography

(Gold) particles

Separation efficiency

ABSTRACT

Although few attempts for classification of nanoparticles (NPs) in lab-scale do exist, the transfer to industrial applications is still challenging. One promising separation method, which is already established for biological molecules, is chromatography. Herein, we study the classification of differently sized gold NPs (AuNPs) by size-exclusion chromatography (SEC). First, we investigated the interactions of AuNPs with potential stationary phases in order to identify a suitable material for the chromatographic process where irreversible NP adhesion is excluded. Then, we demonstrate the high reproducibility of our SEC experiments by multiple sample injections that lead to constant peak areas. In particular, we show the size-dependent elution behavior of AuNP mixtures resulting in bimodal elution peaks, where size separation was confirmed by inline measured UV/Vis spectra. Finally, NP classification results by using a fraction collector are characterized by retention time, mass balances and size-dependent separation efficiencies. The adjustment of the particle size distributions (PSDs) is demonstrated by changing the switching time of the fraction collector. Our study evidences the high potential of SEC for preparative and continuous separation of NPs.

© 2018 The Authors. Published by Elsevier B.V. This is an open access article under the CC BY-NC-ND license (<http://creativecommons.org/licenses/by-nc-nd/4.0/>).

1. Introduction

Particles and especially nanoparticles (NPs) are important materials in various fields ranging from electronics to medicine [1, 2]. However, final product properties are determined not only by the chemical composition, but also by disperse properties, i.e. particle size, shape and morphology [3, 4]. For high-quality products, a defined and narrow particle size distribution (PSD) is desired, since a small change in PSD can have a large impact on their properties, for instance the interaction of NPs with light is strongly size- and shape-dependent. NPs can be produced by top-down (e.g. nanomilling) and bottom-up synthesis in the gas and liquid phase in technically relevant quantities. Most of these techniques produce size-distributed NPs and despite the remarkable

progress in liquid phase syntheses of well-defined NPs of controlled size and shape, a classification step is mandatory to adjust or modify the obtained PSD according to the needs of the later product. Specific targets for the classification are: the separation of a broader feed into two or more fractions, the removal of fine or coarse tail fractions, shape separation, as many NP syntheses lead to shape distributions (e.g. in the case of noble metal nanorods also spheres are obtained), or the separation of by-products when several phases are formed. For instance, a narrowing of the initial PSD or exclusion of an unwanted particle fraction might already significantly improve the NP performance of the later application.

Most technically established classification techniques (e.g. deflector wheel classifiers [5, 6] and gas cyclones [7, 8] in the gas phase or centrifuges [9] and hydrocyclones [7] in the liquid phase) are based on the force balance between the centrifugal force and the drag force acting on the particles and are restricted to particle sizes above 1 µm. Noteworthy, classification of particles >50 nm based on mass forces is challenging but was only achieved recently using a discontinuous tubular-bowl centrifuge with high accelerations up to 40,000 x g [10, 11].

For the classification of NPs, a few techniques like electrophoresis, mobility analysis, analytical ultracentrifugation (AUC) and size-selective precipitation (SSP) do exist [12]. Electrophoresis of NPs is based on the size- and shape-dependent mobility of charged particles in a stationary electrical field. Hanauer et al. showed the separation of silver

Abbreviations: AC, Analytical centrifugation; AgNPs, Silver nanoparticles; AUC, Analytical ultracentrifugation; AuNPs, Gold nanoparticles; CCD, charge-coupled device; DAD, Diode-array detector; FFF, Field-flow fractionation; HPLC, High performance liquid chromatography; ICP-OES, Inductively coupled plasma optical emission spectrometry; NPs, Nanoparticles; PSD, Particle size distribution; QDs, Quantum dots; RCA, Relative centrifugal acceleration; RSD, Relative standard deviation; SEC, Size-exclusion chromatography; SEM, Scanning electron microscope; SMB, Simulated moving bed; SPR, Surface plasmon resonance; SSP, Size-selective precipitation; ST, Switching time; TEM, Transmission electron microscope.

* Corresponding author at: Institute of Particle Technology (LFG), Friedrich-Alexander-Universität Erlangen-Nürnberg (FAU), Cauerstr. 4, 91058 Erlangen, Germany.

E-mail address: Wolfgang.Peukert@fau.de (W. Peukert).

NPs (AgNPs) according to their size and shape by gel electrophoresis [13]. Furthermore, spherical CdSe quantum dots (QDs) were separated from CdSe nanoplatelets due to the higher electrophoretic mobility of the QDs [14]. AUC, a powerful technique in terms of particle size and shape analysis, which we improved in recent years [15, 16], enables the separation of NPs to analyze disperse properties with outstanding resolution. Mastronardi et al. separated SiNPs <10 nm by a density gradient AUC on analytical scale [17]. However, all these techniques are mainly restricted to the lab scale with very small throughput and cannot be used for industrial separation of NPs.

For the classification of particles smaller than 5 nm, Segets et al. [18] used SSP [19, 20] and analyzed separation efficiency and yield. This technique is based on the addition of a second liquid into a colloidal suspension to adjust the van der Waals attraction and thus colloidal stability via the dielectric permittivity of the solvent mixture. When the liquid composition is properly adjusted, due to size-dependent van der Waals attraction, larger particles reversibly flocculate preferentially into structures clearly above the primary particle size that can be easily isolated by preparative centrifugation [21, 22]. At the moment, this method is restricted to a defined set of materials, i.e. semiconductor NPs with strongly adsorbed ligands at the surface, and requires larger quantities of solvent mixtures.

In contrast, chromatographic techniques are well established in biotechnology and polymer science for the separation of macromolecules, e.g. proteins (particle size <10 nm) or viruses (particle size <100 nm), their transfer to industrial scale is possible [23–26]. Furthermore, the potentially aspired continuous operation mode of size-exclusion chromatography (SEC) was recently shown for the purification of antibodies and viruses using Simulated Moving Bed (SMB) chromatography, which led to a higher productivity by a factor of 11 compared to the batch process [27, 28]. In most cases, the isolation of a well-defined target protein with a distinct size is the major goal of the separation.

The separation of NPs is challenging compared to proteins since NP ensembles are typically widely distributed in size and shape while their surface properties are often not sufficiently understood due to physi- and/or chemisorbed ligand species at the surface. Separation via SEC is based on the hydrodynamic volume of particles or molecules, whereat smaller species diffuse further into the porous structure of the stationary phase and thus elute the column later than the larger fraction. SEC is so far mainly used for classification of biopolymers and synthetic polymers [29]. However, the analytical separation of NPs by SEC was already successfully applied [30] and achieved for SiO₂ NPs [31], metal NPs [32, 33] and semiconductor NPs [34] in a size range of 2 nm to 200 nm. In addition, the capability of SEC was demonstrated by shape-selective separation of NPs, e.g. separation of spheres and rods [35] or rods and tetrapods [34]. Recycling size-exclusion chromatography allowed increased resolution of the separation down to below 1 nm in size [33].

Since now, the separation of NPs by SEC is only described qualitatively by retention times and peak resolution but without consideration of mass balances and size-dependent separation efficiencies. Therefore, we herein investigated the classification of AuNPs with different sizes and their mixtures by SEC using an additional fraction collector, which allowed us to collect size-selected fractions in separate vials. This allows us to further analyze the obtained fractions, i.e. coarse and fine fraction, with respect to mass fractions, PSDs and size-dependent separation efficiencies. The quantitative, mass-balance-based evaluation of SEC is mandatory for most industrial applications, which require adjustable cut sizes, high selectivity and yield.

Therefore, we systematically investigate the separation of NPs by SEC starting with the interactions of NPs, mobile phase and stationary phase, in order to prevent NP agglomeration as well as irreversible NP adsorption on the stationary phase. This guarantees an extended use of the SEC column since the porous system is prevented from blockage. We will first confirm the feasibility of NP separation for AuNPs using chromatography and in particular SEC by making use of inline measured

UV/Vis spectra. Then, we investigated the classification of a multimodal AuNP size mixture that resulted into a clear separation into two fractions eluting at different retention times. Finally, we applied evaluation methods from particle technology to SEC in order to describe the size-dependent NP separation quantitatively. Although many open questions are remaining, we conclude that SEC possesses huge potential for the preparative and continuous separation of NPs. General evaluation methods known from particle technology can be used and combined with chromatographic methods in order to get an in-depth understanding of the complex size-dependent classification process. This paves the way towards PSDs truly tailored for the later application.

2. Materials and methods

2.1. Chemicals

2.1.1. Synthesis of AuNPs and SEC experiments

All chemicals used in this study were of analytical purity. For synthesis of citrate capped AuNPs, millipore water (18.2 MΩ cm⁻¹), trisodium citrate dihydrate (Na₃C₆H₅O₇ × 2H₂O, Merck KGaA) and chloroauric acid trihydrate (HAuCl₄ × 3H₂O, Merck KGaA) were used. For SEC experiments, a 7.5 mM monosodium phosphate (NaH₂PO₄, Merck KGaA) buffer was used.

2.1.2. Stationary phases

Two commercially available stationary phases were tested for their application in SEC experiments. First, a silica gel purchased from Carl Roth (stationary phase 1, particle size 85 μm; pore size 15 nm) was used as a representative silica test phase. In addition, a second material (stationary phase 2, mean particle size 10 μm; pore size 100 nm) was provided by PSS Polymer Standards Service GmbH as stationary phase for SEC.

2.2. Methods

2.2.1. Zeta potential and PSD

For analysis of zeta potentials of the initial AuNPs, a Zetasizer Nano ZS (Malvern Instruments) was used. Samples were measured in a disposable electrophoresis cell (DTS 1070, Malvern Instruments). Using the Smoluchowski approach, the determined electrophoretic mobilities were converted to zeta potential. For characterization of synthesized AuNPs and to obtain the PSDs of the coarse and the fine fraction after classification, microscopic techniques were used. For the latter, we used a transmission electron microscope (TEM, Philips CM30 TWIN/STEM (FEI Company, Eindhoven, the Netherlands)) equipped with a LaB₆ filament operated at an acceleration voltage of 300 kV. Images were recorded with a CCD camera (TVIPS GmbH, Gauting, Germany) at five frames per second and an image size of 1024 × 1024 pixels. Samples were trickled and dried on lacey TEM grids (Plano GmbH) prior analysis.

Additionally, analytical centrifugation (AC) was used to determine PSDs of initial AuNP samples with high resolution. Measurements were performed with a LUMiSizer LS 651 (LUM GmbH, Berlin, Germany) at a wavelength λ of 470 nm to maximize the sensitivity against small particles with low scattering. The temperature was set to 20 °C for all measurements and commercially available polycarbonate cells with an optical path length of 2 mm (LUM GmbH, Berlin, Germany) were used. The cuvettes were filled with 430 μl of suspension and inserted into the rotor. Measurements were performed at 4000 rpm corresponding to a relative centrifugal acceleration (RCA) of 2300 at the cell bottom. The measured sedimentation profiles are shown in SI 1. We used an algorithm developed at our institute to calculate the PSD from the sedimentation profiles [36]. The zeta potentials and mean particle sizes (balanced mean/mean number weighted particle size $x_{1,0}$) obtained with the Zetasizer and AC, respectively, are summarized in Table 1.

Table 1

Zeta potential, mean number weighted particle size ($x_{1,0}$), standard deviation σ and relative standard deviation (RSD) of synthesized AuNPs.

Zeta potential/mV	Particle size $x_{1,0}$ /nm	σ /nm	RSD/-
-42.7 ± 0.7	22.2	2.0	0.09
-41.5 ± 1.5	30.2	5.9	0.16
-42.0 ± 0.6	37.6	4.1	0.11
-43.4 ± 0.8	42.3	4.5	0.11

The herein used mean particle size $x_{1,0}$ is defined as the abscissa of the center of gravity by area of the number density distribution q_0 :

$$x_{1,0} = \int_{x_{\min}}^{x_{\max}} x q_0(x) dx \quad (1)$$

In addition, well-known quantities are available from mechanical process engineering to characterize PSDs. These are the standard deviation σ and the relative standard deviation (*RSD*; $RSD = \sigma/x_{1,0}$), which is a dimensionless quantity to characterize the width of a PSD. $RSD < 10\%$ indicates narrow PSDs, whereas $RSD < 5\%$ is usually referred to as “monodisperse”. However, at this point it has to be mentioned that the *RSD* depends on the quantity r based on which the PSD is derived. Thus, *RSD* changes, if e.g. the mode particle size (maximum of the density distribution) or the median particle size (size at which 50% of the particles are smaller) is used, or if the distributions are calculated number based ($r = 0$) or mass based ($r = 3$). For our calculations, we used the balanced mean by number, $x_{1,0}$, since on the one hand, the center of gravity addresses the non-symmetric shape of the PSDs and on the other hand, by choosing number as quantity small and large particles are equally represented.

2.2.2. Mass fraction

For closing the mass balance and to obtain the mass fraction of the coarse and the fines after classification, particle masses in the feed, coarse and fines were determined by inductively coupled plasma optical emission spectrometry (ICP-OES) using an Optima 8300 spectrometer from Perkin Elmer, Inc. After SEC experiments, samples (typically 3 ml) were digested with 400 μ l *aqua regia* and analyzed.

2.2.3. Stability experiments

For the successful implementation of NP separation by SEC, the various interactions of NPs, stationary phase and mobile phase are of major importance. As already mentioned, the principle of SEC is the separation based on the size-dependent diffusion of NPs through the porous stationary phase. Hence, any irreversible NP adsorption on the stationary phase has to be excluded. At this point it has to be mentioned that achieving no interactions between NPs and stationary phase at all, which is in principle desired for SEC, is unlikely. However, exclusion of irreversible attraction is absolutely mandatory, as otherwise stationary phases would be plugged by adsorbed particles. Therefore, we performed shaking experiments in a simple experimental setup in order to quantify the adsorption of AuNPs on potential stationary phases. NPs were mixed with the mobile phase and the stationary phase and put into a shaking rack to guarantee continuous mixing of particles over the whole experimental time and to prevent stationary phase particles from sedimentation (time = t_0). The temperature was kept constant at 20 °C. After settling of the stationary phase particles, the supernatant was analyzed by UV/Vis spectrometry (Cary 100 Scan, Varian) at defined time steps (time = t_x) and compared to the initial sample to check whether the AuNPs did adsorb or not. The shaking experiments were carried out for up to six days to allow for sufficiently long times that NPs can diffuse and potentially adsorb on the porous stationary phase. In addition, with these experiments aggregation/agglomeration of AuNPs induced by the stationary phase particles was investigated. Finally, it has to be mentioned that the effect of marginal

NP adsorption at the vial walls was subtracted by using a blank sample without stationary phase for each time step.

2.2.4. SEC setup

Chromatographic experiments were performed by a UHPLC setup from Thermo Fisher Scientific Inc. containing an auto sampler (ASI 100), a gradient pump (LPG-3400SD), a column oven (STH 585), a diode-array detector (DAD, DAD Ultimate 3000) and a fraction collector (AFC 3000). With this setup, detection of a full extinction spectrum at the retention peak maximum was performed, while samples were collected in separate vials after the detector. The flow rate was set to 1 ml min⁻¹ using a 7.5 mM NaH₂PO₄ buffer.

2.2.5. Data evaluation of SEC separation

In a first instance, all chromatograms were analyzed with respect to well-known chromatographic quantities, namely the retention time t_R , the peak width w_i and the peak area a_i . The resolution of the peak separation R_S of two peaks i and j was evaluated according to [37]:

$$R_S = \frac{2(t_{R,j} - t_{R,i})}{w_i + w_j} \quad (2)$$

In general, a resolution R_S of 1.5 corresponds to a baseline separation, whereas $R_S = 1.0$ indicates a peak overlap of 3% [37]. However, in case of disperse systems as solute, the drawback of this evaluation is the lack of information about the relation between eluate and the actual particle size, or even more precise, the evolution of PSD with retention time.

A generally applicable approach for measuring the success of classification was established in the field of particle technology, especially for the separation of large particles $>1 \mu$ m [7, 38, 39]. Noteworthy, this kind of data evaluation was also applied recently to analyze the classification of small NPs (<5 nm) in liquid phase [18, 21]. Therefore, all samples were analyzed with respect to the PSD and the relative masses of the coarse fraction g and the fine fraction f :

$$g = \frac{m_g}{m_F} \quad (3)$$

$$f = \frac{m_f}{m_F} \quad (4)$$

With the mass of feed m_F , coarse m_g and fines m_f . Herein, the masses were obtained from ICP-OES measurements. Using the PSDs of the feed $q_F(x)$, the coarse $q_g(x)$ and the fines $q_f(x)$ derived from TEM, the separation efficiency $T(x)$ is derived:

$$T(x) = g \frac{q_g(x)}{q_F(x)} = 1 - f \frac{q_f(x)}{q_F(x)} \quad (5)$$

Noteworthy, since $T(x)$ includes the mass balance, it is independent of the quantity r based on which the PSD is derived (e.g. number or volume based). With known $T(x)$, the cut size x_t is determined, describing the particle size which is found equally in the coarse and the fine fraction ($T(x) = 0.5$). Furthermore, to describe the steepness of the cut, similar to *RSD*, the separation sharpness κ is introduced:

$$\kappa = \frac{x_{25,t}}{x_{75,t}} \quad (6)$$

Where $x_{25,t}$ and $x_{75,t}$ are the particle sizes for which $T(x)$ equals 0.25 and 0.75, respectively. Herein, the classification is usually sorted into *ideal* ($\kappa = 1$), *analytical* ($\kappa = 0.8-0.9$), *sharp* ($\kappa = 0.6-0.8$) and *technical* ($\kappa = 0.3-0.6$) for micron-sized particles. Finally, the yields of the coarse η_g and the fines η_f quantify amounts of particles below x_t that went to

the fine fraction (1 in case of an ideal classification) and above x_t that went to the coarse (1 in case of an ideal classification), respectively:

$$\eta_g = \frac{\int_{x_t}^{x_{\max}} [gq_g(x)dx]}{\int_{x_t}^{x_{\max}} [q_F(x)dx]} \quad (7)$$

$$\eta_f = \frac{\int_{x_{\min}}^{x_t} [fq_f(x)dx]}{\int_{x_{\min}}^{x_t} [q_F(x)dx]} \quad (8)$$

3. Results and discussion

3.1. Introduction of classification problem

In the following, we will introduce the classification problem which is regarded to be typical for NPs grown in the liquid phase that are either synthesized by complex multistep protocols and/or produced at larger quantities where concentration and temperature distributions in time and space are difficult to control. For bottom-up synthesis of differently sized AuNPs, a consecutive NP growing routine is often applied. In this study, we used a technique developed by Turkevich et al. in order to synthesize differently sized citrate capped AuNPs [40, 41]. The general procedure is depicted in Fig. 1a. First, 2.2 mM $\text{Na}_3\text{C}_6\text{H}_5\text{O}_7 \times 2\text{H}_2\text{O}$ in 150 ml millipore water ($18.2 \text{ M}\Omega \text{ cm}^{-1}$) was heated and refluxed at 95°C . Afterwards, 1 ml of 25 mM $\text{HAuCl}_4 \times 3\text{H}_2\text{O}$ was injected and the reaction was completed after 10 min (Fig. 1a, step 1). The obtained AuNPs were then used as seeds for the preparation of differently sized AuNPs using a successive growth method [42, 43]. Therefore, the seed suspension was cooled and kept at a temperature of 90°C for the rest of the synthesis, followed by an injection of 1 ml of 25 mM $\text{HAuCl}_4 \times 3\text{H}_2\text{O}$ solution (Fig. 1a, step 2). After 30 min, the injection of 1 ml of 25 mM $\text{HAuCl}_4 \times 3\text{H}_2\text{O}$ was repeated. After three consecutive injections, 55 ml of the reaction dispersion was extracted (Fig. 1a, step 3)

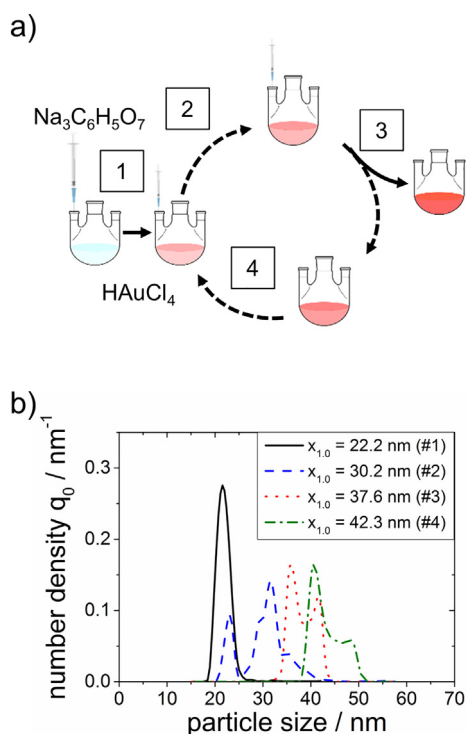


Fig. 1. (a) Consecutive NP growing routine for the synthesis of differently sized AuNPs [42]. (b) PSDs of synthesized AuNPs measured by AC.

and replaced by 53 ml of millipore water and 2 ml of 60 mM $\text{Na}_3\text{C}_6\text{H}_5\text{O}_7 \times 2\text{H}_2\text{O}$ (Fig. 1a, step 4).

The resulting dispersion was then used as seeds for the subsequent growth step. This procedure was repeated three times until four samples (#1–#4) of AuNPs with mean sizes $x_{1,0}$ between 22.2 (#1) and 42.3 nm (#4) were synthesized (scanning electron microscope (SEM) images and extinction spectra are shown in SI 2). However, due to the sequential growth steps where any imperfections in the previous step are input for the subsequent reaction, dispersity accumulates and a broadening of the PSDs with increasing synthesis cycles is inevitable. This is confirmed by the number weighted PSDs measured by AC shown in Fig. 1b. First, in line with the expectations, PSDs of AuNPs shift to larger particle sizes with each synthesis step. However, with increasing cycles, an additional broadening of the PSD as well as multimodalities are observed. This is also reflected by *RSD*, which increases from 0.09 in case of cycle #1 to 0.16 for cycle #2, 0.11 for cycle #3 and finally 0.11 for cycle 4. In order to adjust the samples for the later application and in particular when thinking on larger scale processes for NP synthesis that will inevitably cause dispersity, a post-synthetic separation or narrowing of the PSDs is absolutely mandatory. Hence, the question arises whether or not SEC can potentially be used to narrow down the dispersity of those AuNPs demonstrating its potential for classification of NPs on technical scale.

3.2. Interactions of NPs and stationary phase

As already mentioned, the interactions between AuNPs and stationary phase materials play a major role for the success of NP separation by SEC. Prior any SEC experiments, we investigated the adsorption of AuNPs ($x_{1,0} = 22.2 \text{ nm}$) on potential stationary phases using shaking experiments. Additionally, those studies allowed conclusions on the long-term stability of NPs against agglomeration in contact with stationary phases. Fig. 2 shows the time-dependent normalized extinction *E* of AuNPs at a wavelength of 520 nm for the adsorption experiments on stationary phase 1 and stationary phase 2. As can be seen, for the stationary phase 2 (Fig. 2, black squares) the normalized extinction of AuNPs stays almost constant over the whole experimental time of six days.

In contrast, the AuNPs clearly adsorb at stationary phase 1 (SiO_2 , Fig. 2, blue circles) already after two days. This phase cannot be used for the chromatographic separation of AuNPs, since particles will block the pores. Thus, we chose stationary phase 2 packed in a chromatography column for all SEC separation experiments described in the following. Noteworthy, the concept of shaking experiments can be parallelized, in order to screen potential stationary phases for the use in SEC with higher throughput. In the next step, we performed a first series of SEC experiments to examine reproducibility and to show the detectability

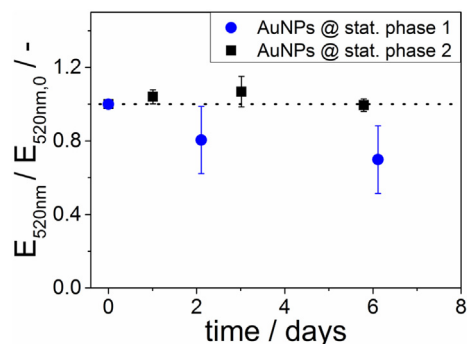


Fig. 2. Normalized extinction over six days during shaking experiments of AuNPs (#1: $x_{1,0} = 22.2 \text{ nm}$) in contact with stationary phase 1 particles (blue circles) and stationary phase 2 particles (black squares).

of AuNPs by the HPLC-setup. In particular, reproducibility is of major importance when quantitative data on classification is strived for.

3.3. Reproducibility of SEC experiments

To examine reproducibility, we investigated the elution behavior of AuNPs (#2 where already slight bimodality does occur with $x_{1,0} = 30.2$ nm, $c_{30.2 \text{ nm}} = 5.5 \times 10^{11}$ NPs ml⁻¹) by performing two individual series of three consecutive injections of 30 µl AuNPs at a flow rate of 1 ml min⁻¹ using 7.5 mM NaH₂PO₄ as mobile phase. The obtained chromatograms are shown in Fig. 3a. Six identical peaks on top of each other at a retention time maximum of 5.6 min clearly show detectability of AuNPs and high reproducibility of the performed SEC measurements. As already mentioned in Section 2.2.3, irreversible NP adsorption on the stationary phase needs to be excluded. To further address this important aspect and to confirm our results from the adsorption experiments, the peak areas of three independent injections are plotted in Fig. 3b. The three injections clearly show nearly identical peak areas (deviation of 0.8%) meaning if adsorption takes place it is negligible and within the experimental scatter of UV/Vis analyses. This again confirms our previous findings from the shaking experiments and justifies our decision for

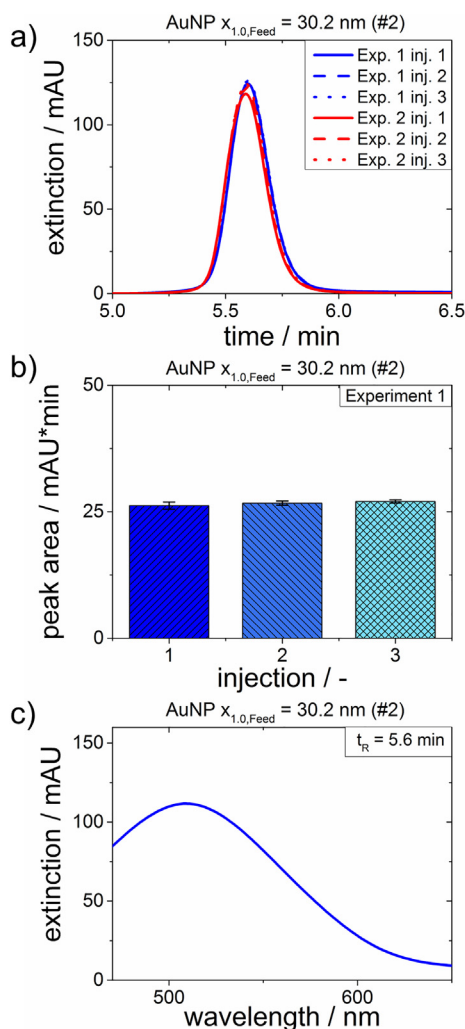


Fig. 3. (a) Chromatograms of AuNPs (#2: $x_{1,0} = 30.2$ nm) for six independent injections of 30 µl AuNPs suspension at a flow rate of 1 ml min⁻¹ using 7.5 mM NaH₂PO₄ as mobile phase and a detection wavelength of 520 nm. Each set of three injections (Exp. 1 in blue and Exp. 2 in red, respectively) was performed at different days after completely restarting the SEC setup. (b) Peak areas and standard deviations of three individual injections for AuNPs of Exp. 1. (c) Extinction spectrum at the retention peak maximum at 5.6 min.

stationary phase 2. In general, the high reproducibility of SEC experiments gives confidence for the following studies, since it shows the significance and reliability of the obtained results. Furthermore, the inline recorded extinction spectrum at the retention peak maximum (t_R) of the chromatogram depicts the typical extinction profile of AuNPs with a surface plasmon resonance (SPR) peak at 510 nm (Fig. 3c). This confirms not only the high reproducibility but also detectability of AuNPs in the SEC experiments, which will be discussed in more detail in the following.

3.4. SEC of differently sized AuNPs

After showing the feasibility and reproducibility of the SEC experiments, we investigated the effect of particle size on the elution behavior. Therefore, all AuNP samples with smaller and larger mean particle sizes ($x_{1,0} = 22.2$ nm – $x_{1,0} = 42.3$ nm) were used (note that at constant mass concentration the number concentration varies from $c_{22.2 \text{ nm}} = 1.1 \times 10^{12}$ NPs ml⁻¹, $c_{30.2 \text{ nm}} = 5.5 \times 10^{11}$ NPs ml⁻¹, $c_{42.3 \text{ nm}} = 3.4 \times 10^{11}$ NPs ml⁻¹), a flow rate of 1 ml min⁻¹ and an injection volume of 30 µl was set using 7.5 mM NaH₂PO₄ as mobile phase. The obtained chromatograms normalized to the extinction maximum at 520 nm are shown in Fig. 4a. Noteworthy, normalization was performed to visualize the size-dependent elution as the detector signal of the different AuNPs varies due to the size-dependent extinction (refer to SI 3).

The chromatograms clearly show a significant shift to smaller retention times from 5.65 min to 5.54 min with increasing particle diameter. These results are consistent with expectations for SEC, i.e. larger particles are less able to diffuse into smaller pores of the stationary phase and thus elute earlier compared to the smaller AuNPs.

In addition, this finding is confirmed by the inline measured extinction spectra at the different retention peak maxima shown in Fig. 4b. With increasing particle size, the maximum of the wavelength λ_{max} slightly shifts to larger wavelengths (red shift; $\lambda_{max, 22.2 \text{ nm}} = 507$ nm, $\lambda_{max, 42.3 \text{ nm}} = 515$ nm). This fits to the general theory and expectations for optical properties of differently sized AuNPs governed by size-

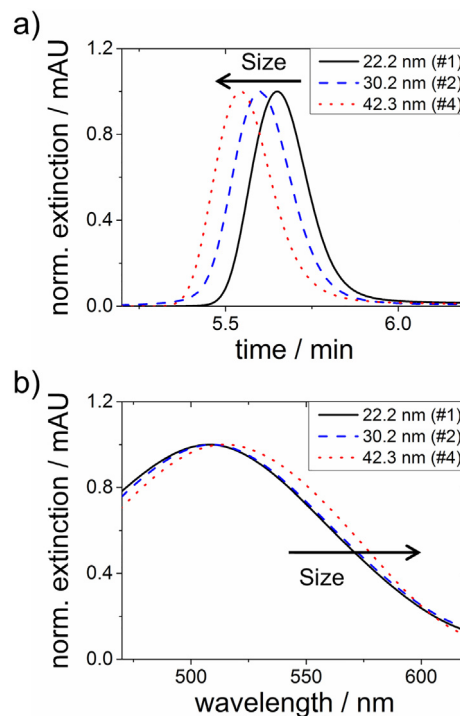


Fig. 4. (a) Normalized chromatograms of differently sized AuNPs ($x_{1,0} = 22.2$ nm – $x_{1,0} = 42.3$ nm) obtained at a flow rate of 1 ml min⁻¹, an injection volume of 30 µl and 7.5 mM NaH₂PO₄ as mobile phase. (b) Extinction spectra at the retention peak maximum exhibiting λ_{max} between 507 and 515 nm for differently sized AuNPs.

dependent surface plasmon resonances in such way that the extinction of larger particles is red shifted (exemplarily, extinction spectra of feed AuNPs and spectra calculated by *MiePlot* are shown in SI 4). Hence, the general application of SEC to NPs seems to be promising since the expected size-dependent trend of elution behavior was observed and confirmed by size-dependent optical properties. In the next step, based on these results the separation of NP mixtures was investigated, where a multimodal distribution was generated by mixing of suspensions #1 and #3 ($x_{1,0} = 22.2$ nm and $x_{1,0} = 37.6$ nm, respectively).

3.5. SEC of AuNP mixtures containing different sizes

To further investigate the separation of AuNPs by SEC, we exemplarily prepared multimodal PSDs consisting of two mean particle sizes (equal volumetric mixing of #1 with $x_{1,0} = 22.2$ nm and #3 with $x_{1,0} = 37.6$ nm, initial particle concentration $c_{22.2 \text{ nm}} = 1.1 \times 10^{12}$ NPs ml^{-1} , $c_{37.6 \text{ nm}} = 4.8 \times 10^{11}$ NPs ml^{-1} ; final particle concentration $c_{22.2 \text{ nm}} = 5.5 \times 10^{11}$ NPs ml^{-1} , $c_{37.6 \text{ nm}} = 2.4 \times 10^{11}$ NPs ml^{-1}), in order to check whether the particles can be separated by their size. We set a flow rate of 1 ml min^{-1} , an injection volume of $30 \mu\text{l}$ and used a NaH_2PO_4 buffer solution (7.5 mM) as mobile phase. The resulting chromatogram and the inline spectra recorded at the peak maxima are depicted in Fig. 5a and b, respectively. The chromatogram clearly shows two distinct, baseline-separated retention time peaks, although the PSD of sample #3 is bimodal, which might be due to the low injection volume. Again the inline spectra recorded at the retention peak maxima clearly hint to the presence of differently sized AuNPs, meaning the first retention time peak ($t_R = 4.9$ min, black circle) refers to larger AuNPs ($x_{1,0} = 37.6$ nm; $\lambda_{\text{max}} = 513$ nm) and the second retention time peak ($t_R = 5.6$ min, red dashed circle) refers to the smaller AuNPs ($x_{1,0} = 22.2$ nm; $\lambda_{\text{max}} = 511$ nm), since the typical red shift of larger particles is observed (for PSDs of the initial samples refer to Fig. 1b).

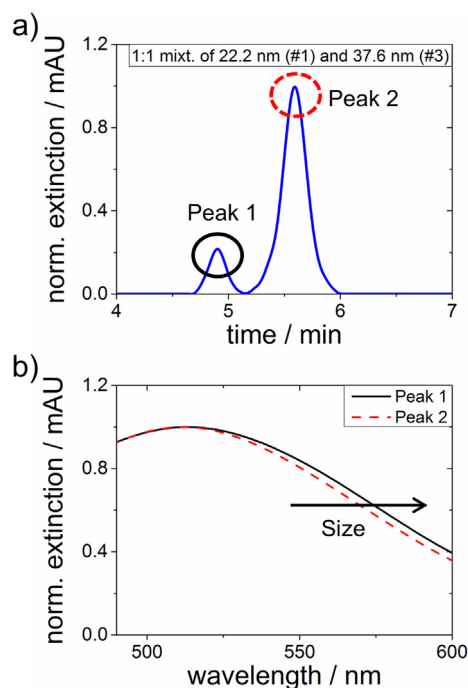


Fig. 5. (a) Chromatogram of a multimodal AuNP mixture (#1 with $x_{1,0} = 22.2$ nm and #3 with $x_{1,0} = 37.6$ nm; final particle concentration $c_{22.2 \text{ nm}} = 5.5 \times 10^{11}$ NPs ml^{-1} , $c_{37.6 \text{ nm}} = 2.4 \times 10^{11}$ NPs ml^{-1}) with a flow rate of 1 ml min^{-1} , an injection volume of $30 \mu\text{l}$ and 7.5 mM NaH_2PO_4 as mobile phase. Black and red dashed circles indicate peak 1 and peak 2, respectively. (b) Inline extinction spectra recorded at the peak maxima of the first peak (black line) and the second peak (red dashed line).

To elucidate this further, we calculated the extinction spectra by *MiePlot* for the measured particle sizes and compared them to the measured extinction spectra (SI 4). As expected, the peak maxima of the calculated spectra are located at smaller wavelengths compared to the measured ones. This is because for the calculations the mean particle size was used, neglecting the polydispersity of the actual PSD and thus the presence of larger particles. Besides, the typical red shift of larger particles is clearly observed in the same order of magnitude as found during SEC experiments. However, although a difference in size of 15 nm does exist, already the optical properties of the feed fractions are quite similar (cf. calculations of extinction spectra via *MiePlot* in SI 4) impeding the quantitative evaluation of particle size based on the optical response only. Therefore, a quantitative analysis of the underlying PSD is absolutely mandatory to judge whether or not SEC is a competitive strategy for NP classification although already from the chromatograms first conclusions can be drawn. A resolution of $R_S = 1.8$ for the separation was derived. For analytical separation a resolution of >1.5 is desired, resulting in a complete baseline separation. Thus, our results give strong hints that a complete baseline separation of NPs by SEC is potentially possible, in particular when process parameters like flow rates and injection volumes as well as the column material will be carefully adjusted and optimized in future works.

3.6. Determination of the fractional separation efficiency

After showing the general applicability of SEC for NPs, we used a fraction collector to separate the initial sample of a multimodal AuNP mixture (monomodal fraction #1 with $x_{1,0} = 22.2$ nm and bimodal fraction #4 with $x_{1,0} = 42.3$ nm) into two different vials. By doing so, the two separate fractions were analyzed in terms of mass and PSD by ICP-OES and TEM, respectively, in order to calculate the size-dependent separation efficiency. This is necessary to quantify the classification independent of the quantity (e.g. number, area, volume) that is used for the derivation of the PSD. Fig. 6a shows the chromatogram with four visible peaks of an AuNP mixture (equal volumetric mixing of $x_{1,0} = 22.2$ nm and $x_{1,0} = 42.3$ nm; initial particle concentration $c_{22.2 \text{ nm}} = 1.1 \times 10^{12}$ NPs ml^{-1} , $c_{42.3 \text{ nm}} = 3.4 \times 10^{11}$ NPs ml^{-1} ; final particle concentration $c_{22.2 \text{ nm}} = 5.5 \times 10^{11}$ NPs ml^{-1} , $c_{42.3 \text{ nm}} = 1.7 \times 10^{11}$ NPs ml^{-1}) using a flow rate of 1 ml min^{-1} , an injection volume of $150 \mu\text{l}$ and a 7.5 mM NaH_2PO_4 buffer solution as mobile phase. Noteworthy, at first glance, the bimodal chromatogram seems to be in line with the expectations due to the multimodalities in PSD of the single AuNP samples (cf. Fig. 1b). However, the separation into four peaks rather likely occurs due to the significantly increased injection volume (see SI 5), as small injection volumes of all four fractions constantly led to single peaks. However, the exact reasons for this concentration-dependent splitting into multimodal chromatograms are beyond the scope of this work and have to be addressed in future studies. For the time being, we would like to discuss the chromatogram in terms of two main peaks with modal values for the retention time maxima whereat the first main peak contains three smaller maxima. To quantify the quality of the cut, we evaluated the retention times of the main peaks to $t_{R,1} = 6.0$ min and $t_{R,2} = 8.4$ min. A peak resolution of $R_S = 1.2$ was observed indicating two separate peaks, however without baseline separation and an overlap of $<3\%$ [7].

For further analysis of the separation, AuNPs were collected into two separate vials using the fraction collector. We set the switching time (ST) of the fraction collector to the minimum of the two main peaks (7.2 min, ST1, blue vertical solid line in Fig. 6a). This led to a total collection time of 5.4 min. In order to describe the separation quantitatively by the separation efficiency explained in Section 2.2, the masses and PSDs of all fractions were evaluated by ICP-OES and TEM, respectively. This more demanding procedure was necessary, since the particle concentration after SEC is too low for analysis via weighing and AC. The calculated mass fractions are summarized in SI 6, though, the total error in terms of the global mass balance is 23% ($g = 0.46$, $f = 0.31$). However, as

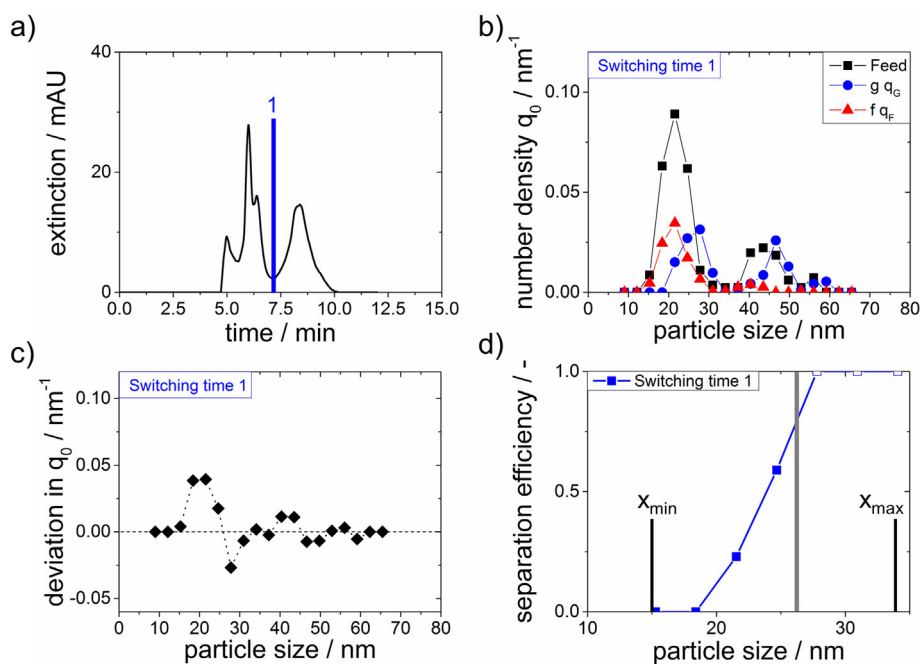


Fig. 6. (a) Chromatogram of AuNP mixture (#1 with $x_{1,0} = 22.2$ nm and #4 with $x_{1,0} = 42.3$ nm) with a flow rate of 1 ml min^{-1} , an injection volume of $150 \mu\text{l}$ and a $7.5 \text{ mM Na}_2\text{HPO}_4$ buffer solution. The blue vertical solid line indicates the switching time (ST) of the fraction collector, i.e. after 7.2 min the vials were changed. (b) Determined PSDs by TEM of feed (black squares), coarse (blue circles) and fines (red triangles) for ST1. (c) Calculated deviation in q_0 of PSDs for SEC experiment with ST1. (d) Evolution of separation efficiency derived from the PSD of the small fraction shown in (b) using SEC in combination with the fraction collector. The grey vertical line indicates the particle size at which the fractional error due to TEM statistics and mass balance is too large and values beyond are not included in the discussion.

repeated experiments confirmed that this error is both, positive and negative, and due to the previously conducted intense studies on reproducibility, we think that this is not caused by significant adsorption of AuNPs at the column material but rather due to the low absolute gold concentration which is situated close to the detection limit of ICP-OES. In future studies, we will overcome this detection limit by using higher concentrations or optically more active materials like colloidal quantum dots.

The resulting number weighted PSDs of the initial AuNPs as well as the coarse and fine fraction are depicted in Fig. 6b (for TEM images refer to SI 7). A clear difference of coarse and fines was observed, while RSDs are slightly decreased in comparison to the feed ($RSD_{Feed} = 0.39$; $RSD_{Coarse} = 0.33$; $RSD_{Fines} = 0.29$) indicating a narrowing of the PSD. Not surprisingly, there is still misclassified material, i.e. small particles in the coarse and large particles in the fine fraction. In addition to errors in mass fractions and PSDs due to detection limits of ICP-OES and TEM statistics, respectively, this is inevitable due to the stochastic nature of diffusion: few larger particles might stay longer in the pores, while a remarkable portion of smaller particles elutes faster than the mean. The only question arises to what extent such oversized particles do occur and how their amount can be minimized. Whereas the former aspect will be discussed in the following, the latter has to be addressed in more detail by future studies.

From the PSDs derived by TEM micrographs, two different size fractions were clearly distinguishable (Fig. 6b). While the larger was not noticeably affected by SEC which could be also due to the small masses and poor statistics, i.e. error typically occurring at the edges of the distribution where the mass balance is hardly closed (see Fig. 6c) [44, 45], the smaller size fraction evidenced clear shifts in the distributions of feed, coarse and fines. Thus, we evaluated the separation efficiency within the boundaries of the smaller size fraction with $x_{\min} = 15.3$ nm and $x_{\max} = 34.0$ nm which are depicted by vertical black lines in Fig. 6d. Although the amount of analyzable size intervals is limited because of the limited number of particles evaluated by TEM (540 particles), a classification effect is clearly recognized. From the PSDs shown in Fig. 6b, a cut

size of $x_t = 23.9$ nm is derived, which is larger than the mode size of the small fraction in the feed distribution ($x_{mod} = 21.5$ nm). Although the number of measurement points is clearly limited, from the evolution of separation efficiency, it already becomes clear that the separation sharpness is very high, with $>80\%$ in the range of an analytical separation when using the current notation for particles $>1 \mu\text{m}$. Remarkably, even narrow feed PSDs can be classified which are intrinsically related to high values for the separation sharpness. Finally, yields of about 43% for the coarse and 33% for the fines were observed which should be understood in terms of their order of magnitude only due to the aforementioned uncertainties (small concentrations, limited statistics due to TEM). Thus, they already evidence the high potential of NP chromatography.

3.7. Adjustment of cut size by variation of the switching time of the fraction collector

Until now, we showed the reproducibility of SEC experiments for separation of AuNPs and discussed the quantitative description of classification by concepts known from chromatography as well as particle technology. Finally, to show the strength of SEC as a reliable method for the separation of NPs, we varied the ST of the fraction collector in order to adjust the cut size of the obtained separation. Therefore, we again analyzed the two separate fractions in terms of mass and PSD and calculated the size-dependent separation efficiency. Fig. 7a shows the chromatogram of the same AuNP mixture used before (#1 with $x_{1,0} = 22.2$ nm and #4 with $x_{1,0} = 42.3$ nm; equal volumetric mixing of $x_{1,0} = 22.2$ nm and $x_{1,0} = 42.3$ nm; initial particle concentration $c_{22.2 \text{ nm}} = 1.1 \times 10^{12} \text{ NPs ml}^{-1}$, $c_{42.3 \text{ nm}} = 3.4 \times 10^{11} \text{ NPs ml}^{-1}$; final particle concentration $c_{22.2 \text{ nm}} = 5.5 \times 10^{11} \text{ NPs ml}^{-1}$, $c_{42.3 \text{ nm}} = 1.7 \times 10^{11} \text{ NPs ml}^{-1}$), derived under the same chromatographic conditions as before (flow rate of 1 ml min^{-1} , an injection volume of $150 \mu\text{l}$ and a $7.5 \text{ mM Na}_2\text{HPO}_4$ buffer solution as mobile phase).

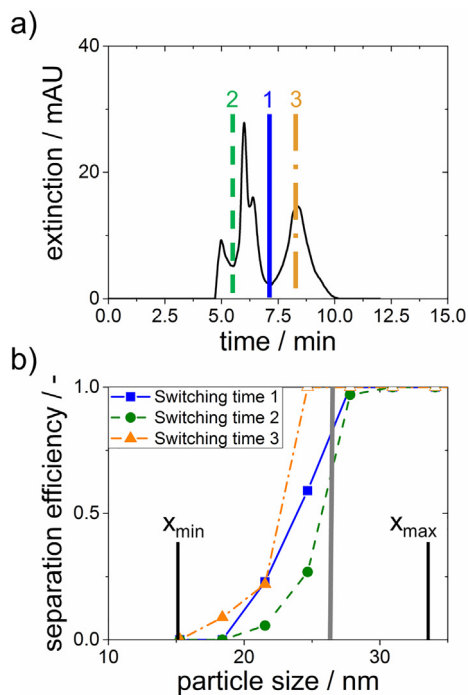


Fig. 7. (a) Chromatogram of AuNP mixture (#1 with $x_{1,0} = 22.2$ nm and #4 with $x_{1,0} = 42.3$ nm) with a flow rate of 1 ml min^{-1} , an injection volume of $150 \mu\text{l}$ and a 7.5 mM NaH_2PO_4 buffer solution. The vertical lines indicate three different ST1–3 of the fraction collector. (b) Separation efficiency curves derived from PSDs for the smaller particle size fraction shown in SI 8 using SEC and the fraction collector for three different STs. The grey vertical line indicates the particle size at which the fractional error due to TEM statistics and mass balance is too large and values beyond are not included in the discussion.

The vertical lines and numbers (blue solid (1), green dashed (2) and orange dashed dotted (3)) in Fig. 7a indicate the STs of the fraction collector at 5.5 min, 7.2 min and 8.3 min, respectively. The resulting PSDs of the initial AuNPs as well as the coarse and fine fraction for ST2 and ST3 are depicted in SI 8. As already discussed along ST1 (Fig. 7a, blue vertical solid line), also in case of ST2 and ST3 a clear change of both, the coarse and the fine fraction, was observed, while the *RSD* is again slightly decreased compared to the feed ($RSD_{Feed} = 0.39$; $RSD_{Coarse,2} = 0.31$; $RSD_{Fines,2} = 0.25$; $RSD_{Coarse,3} = 0.32$; $RSD_{Fines,3} = 0.30$) indicating a narrowing of the PSD.

Similar to the experiment in the previous section, noticeable classification was only observed in the small particle size fraction. The derived curves for the separation efficiency ($x_{min} = 15.3$ nm, $x_{max} = 34.0$ nm) are shown in Fig. 7b (for mass fractions refer to SI 6; for PSDs refer to SI 8). Even though the amount of analyzable size intervals is small, the separation efficiency indicates a clear dependence on the ST. For an early ST (ST2) the separation efficiency curve is shifted to larger particle sizes whereas for a later ST the separation efficiency curve is shifted to smaller particle sizes. This is in line with our expectations, since an early ST (ST2) decreases the number of smaller particles in the early eluting coarse fraction. Vice versa, a later ST (ST3) increases the number of smaller particles in the coarse fraction resulting into a decreased cut size. This depicts how the cut size can potentially be tailored by simply varying the ST.

Accordingly, by analysis of masses and PSDs of AuNPs, we showed the challenges (low particle concentration due to dilution) as well as the large potential (baseline separation, adjustment of cut size) of NP separation using SEC. To the best of our knowledge, this is the first report combining chromatography and evaluation methods from particle technology in order to quantitatively describe the separation of NPs by SEC. Our work demonstrates that SEC is a promising technique for the continuous, post-synthetic classification of NPs on a technical scale, in

order to narrow or tune the PSD. This paves the way for further studies to improve the separation of NPs by SEC in order to obtain desired particle systems with optimized properties for the later application.

4. Summary and conclusion

In this study we showed the applicability of size-exclusion chromatography (SEC) to separate nanoparticles (NPs) with different sizes using quantitative evaluation methods from the field of particle technology. First, we implemented stability experiments to investigate the adsorption behavior of gold NPs (AuNPs) on potential stationary phases. After selecting an appropriate material for the stationary phase, experiments were carried out to show the detectability of AuNPs by SEC with high reproducibility. Afterwards, it was proven that elution follows the general principle of SEC as injection of differently sized AuNPs resulted in enhanced elution times with decreasing particle size. This is because smaller particles are diffusing into the smaller pores of the stationary phase while larger particles move faster through the column. In the next step, a mixture of AuNPs containing two different sizes was investigated resulting in two baseline separated peaks. The separation of a multimodal AuNP mixture into two fractions was realized using a fraction collector. By analyzing the obtained fractions with respect to PSD and mass, for the first time a quantitative evaluation of NP classification by SEC was achieved using the separation efficiency $T(x)$. Noteworthy, this approach is well-known in the field of particle technology, however, usually not applied to chromatographic separation. Finally, we adjusted different PSDs and cut sizes by changing the switching time of the fraction collector demonstrating the potential of SEC for the post-synthetic tuning of disperse systems. Our results show that although many open questions in terms of characterization and identification of optimum process conditions are remaining, SEC is applicable for the classification and post-synthetic narrowing of the dispersity of colloidal NPs. In comparison to other methods like field-flow fractionation (FFF), SEC is in principle a preparative process with a continuous operation mode, i.e. simulated moving bed (SMB) chromatography.

Symbols

Latin symbols

a	Peak area mAU	min
c	Particle concentration	ml^{-1}
E	Extinction	–
f	Fine fraction	–
g	Coarse fraction	–
m	Mass	g
m_F	Mass of feed	g
m_f	Mass of fines	g
m_g	Mass of coarse	g
q_0	Number density distribution	nm^{-1}
q_f	Number density distribution of fines	nm^{-1}
q_F	Number density distribution of feed	nm^{-1}
q_g	Number density distribution of coarse	nm^{-1}
r	Quantity	–
R_S	Resolution	–
t	Time	min
t_R	Retention time	min
$T(x)$	Separation efficiency	–
w	Peak width	s
$x_{1,0}$	Balanced mean/mean number weighted particle size	nm
$x_{25,t}$	Particle size for $T(x)$	0.25 nm
$x_{75,t}$	Particle size for $T(x)$	0.75 nm
x_{mod}	Mode particle size	nm
x_t	Cut size	nm

Greek symbols

η	Yield	–
κ	Separation sharpness	–
λ	Wavelength	nm
σ	Standard deviation	nm

Acknowledgment

The authors acknowledge financial support by the Deutsche Forschungsgemeinschaft (DFG) within the priority program SPP 2045 (PE427/Project C8). Moreover, we acknowledge the Federal Ministry of Economic Affairs and Energy through the Arbeitsgemeinschaft industrieller Forschungsvereinigungen “Otto von Guericke” e.V. (AiF, project no. 18037 N). Furthermore, we thank Prof. Thuerich Hofe from PSS Polymer Standards Service GmbH for providing samples of stationary phases and helpful discussions. Moreover, we thank Patrick Herre for providing TEM images and Dr. Jochen Schmidt for ICP-OES measurements. Additionally, we thank Dr. Johannes Walter for help with AC data analysis.

Appendix A. Supplementary data

Supplementary data to this article can be found online at <https://doi.org/10.1016/j.powtec.2018.08.008>.

References

- [1] S.E. Lohse, C.J. Murphy, Applications of colloidal inorganic nanoparticles: from medicine to energy, *J. Am. Chem. Soc.* 134 (2012) 15607–15620.
- [2] T. Minari, Y. Kanehara, C. Liu, K. Sakamoto, T. Yasuda, A. Yaguchi, S. Tsukada, K. Kashizaki, M. Kanehara, Room-temperature printing of organic thin-film resistors with π -junction gold nanoparticles, *Adv. Funct. Mater.* 24 (2014) 4886–4892.
- [3] H. Rumpf, Über die Eigenschaften von Nutztstäuben, *Staub Reinh. Luft* (1967) 3–13.
- [4] W. Peukert, D. Segets, L. Pflug, G. Leugering, Unified design strategies for particulate products, in: G.B. Marin, J. Li (Eds.), *Advances in Chemical Engineering, Mesoscale modeling in chemical engineering*, vol. 46, Academic Press, Amsterdam, Boston, Heidelberg 2015, pp. 1–81.
- [5] M. Stender, K. Legenhausen, A.P. Weber, Visualisierung der Partikelbewegung in einem Abweiseradsichter, *Chem. Ing. Tech.* 87 (2015) 1392–1401.
- [6] J. Galk, W. Peukert, J. Krahn, Industrial classification in a new impeller wheel classifier, *Powder Technol.* 105 (1999) 186–189.
- [7] H. Schubert, *Handbuch der Mechanischen Verfahrenstechnik*, Wiley-VCH, 2002.
- [8] J. Galk, W. Peukert, Cyclone classifier for inline- and offline-classification, *Powder Handl. Process.* 8 (1996) 55–58.
- [9] S. Stahl, L.-E. Spelter, H. Nirschl, Investigations on the separation efficiency of tubular bowl centrifuges, *Chem. Eng. Technol.* 31 (2008) 1577–1583.
- [10] L.E. Spelter, H. Nirschl, Classification of fine particles in high-speed centrifuges, *Chem. Eng. Technol.* 33 (2010) 1276–1282.
- [11] M. Konrath, A.-K. Brenner, E. Dillner, H. Nirschl, Centrifugal classification of ultrafine particles: influence of suspension properties and operating parameters on classification sharpness, *Sep. Purif. Technol.* 156 (2015) 61–70.
- [12] Y. Mori, Size-Selective Separation Techniques for Nanoparticles in Liquid, *KONA Powder Part. J.* (2015) 102–114.
- [13] M. Hanauer, S. Pierrat, I. Zins, A. Lotz, C. Sönnichsen, Separation of nanoparticles by gel electrophoresis according to size and shape, *Nano Lett.* 7 (2007) 2881–2885.
- [14] E. Lhuillier, P. Hease, S. Ithurria, B. Dubertret, Selective electrophoretic deposition of CdSe Nanoplatelets, *Chem. Mater.* 26 (2014) 4514–4520.
- [15] J. Walter, P.J. Sherwood, W. Lin, D. Segets, W.F. Stafford, W. Peukert, Simultaneous analysis of hydrodynamic and optical properties using analytical ultracentrifugation equipped with multiwavelength detection, *Anal. Chem.* 87 (2015) 3396–3403.
- [16] J. Walter, W. Peukert, Dynamic range multiwavelength particle characterization using analytical ultracentrifugation, *Nanoscale* 8 (2016) 7484–7495.
- [17] M.L. Mastronardi, F. Hennrich, E.J. Henderson, F. Maier-Flaig, C. Blum, J. Reichenbach, U. Lemmer, C. Kübel, M.M. Kappes Di Wang, G.A. Ozin, Preparation of monodisperse silicon nanocrystals using density gradient ultracentrifugation, *J. Am. Chem. Soc.* 133 (2011) 11928–11931.
- [18] D. Segets, S. Komada, B. Butz, E. Spiecker, Y. Mori, W. Peukert, Quantitative evaluation of size selective precipitation of Mn-doped ZnS quantum dots by size distributions calculated from UV/Vis absorbance spectra, *J. Nanopart. Res.* 15 (2013) 1111.
- [19] T. Vossmeier, L. Katsikas, M. Giersig, I.G. Popovic, K. Diesner, A. Chemseddine, A. Eychemueller, H. Weller, CdS nanoclusters: synthesis, characterization, size dependent oscillator strength, temperature shift of the excitonic transition energy, and reversible absorbance shift, *J. Phys. Chem.* 98 (1994) 7665–7673.
- [20] C.B. Murray, D.J. Norris, M.G. Bawendi, Synthesis and characterization of nearly monodisperse CdE (E = sulfur, selenium, tellurium) semiconductor nanocrystallites, *J. Am. Chem. Soc.* 115 (1993) 8706–8715.
- [21] D. Segets, C. Lutz, K. Yamamoto, S. Komada, S. Stieß, Y. Mori, W. Peukert, Classification of zinc sulfide quantum dots by size: insights into the particle surface–solvent interaction of colloids, *J. Phys. Chem. C* 119 (2015) 4009–4022.
- [22] M.L. Mastronardi, F. Maier-Flaig, D. Faulkner, E.J. Henderson, C. Kübel, U. Lemmer, G. A. Ozin, Size-dependent absolute quantum yields for size-separated colloidal-stable silicon nanocrystals, *Nano Lett.* 12 (2012) 337–342.
- [23] R. Ghosh, Protein separation using membrane chromatography: opportunities and challenges, *J. Chromatogr. A* 952 (2002) 13–27.
- [24] A. Podgornik, S. Yamamoto, M. Peterka, N.L. Krajnc, Fast separation of large biomolecules using short monolithic columns, *J. Chromatogr. B* 927 (2013) 80–89.
- [25] R. Morenweiser, Downstream processing of viral vectors and vaccines, *Gene Ther.* 12 (Suppl. 1) (2005) S103–S110.
- [26] S. Swernath, M. Kaspareit, A. Kienle, Coupled continuous chromatography and racemization processes for the production of pure enantiomers, *Chem. Eng. Technol.* 37 (2014) 643–651.
- [27] C.A. Martinez Cristancho, A. Seidel-Morgenstern, Purification of single-chain antibody fragments exploiting pH-gradients in simulated moving bed chromatography, *J. Chromatogr. A* 1434 (2016) 29–38.
- [28] T. Krober, M.W. Wolff, B. Hundt, A. Seidel-Morgenstern, U. Reichl, Continuous purification of influenza virus using simulated moving bed chromatography, *J. Chromatogr. A* 1307 (2013) 99–110.
- [29] M. Gaborieau, P. Castignolles, Size-exclusion chromatography (SEC) of branched polymers and polysaccharides, *Anal. Bioanal. Chem.* 399 (2011) 1413–1423.
- [30] B. Kowalczyk, I. Lagzi, B.A. Grzybowski, Nanoseparations: strategies for size and/or shape-selective purification of nanoparticles, *Curr. Opin. Colloid Interface Sci.* 16 (2011) 135–148.
- [31] Z. Aspanut, T. Yamada, L.W. Lim, T. Takeuchi, Light-scattering and turbidimetric detection of silica colloids in size-exclusion chromatography, *Anal. Bioanal. Chem.* 391 (2008) 353–359.
- [32] F. Liu, G. Wei, Effect of mobile-phase additives on separation of gold nanoparticles by size-exclusion chromatography, *Chromatographia* (2004) 115–119.
- [33] A.M. Al-Somali, K.M. Krueger, J.C. Falkner, V.L. Colvin, Recycling size exclusion chromatography for the analysis and separation of nanocrystalline gold, *Anal. Chem.* 76 (2004) 5903–5910.
- [34] K.M. Krueger, A.M. Al-Somali, J.C. Falkner, V.L. Colvin, Characterization of nanocrystalline CdSe by size exclusion chromatography, *Anal. Chem.* 77 (2005) 3511–3515.
- [35] G.-T. Wei, F.-K. Liu, Separation of nanometer gold particles by size exclusion chromatography, *J. Chromatogr. A* 836 (1999) 253–260.
- [36] J. Walter, T. Thajudeen, S. Stieß, D. Segets, W. Peukert, New possibilities of accurate particle characterisation by applying direct boundary models to analytical centrifugation, *Nanoscale* 7 (2015) 6574–6587.
- [37] H. Schmidt-Traub, *Preparative Chromatography of Fine Chemicals and Pharmaceutical Agents*, Wiley-VCH, Weinheim, 2005.
- [38] K. Leschonski, Kennzeichnung disperster Systeme, *Teilchengrößenanalyse*, *Chem. Ing. Tech.* 45 (1973) 8–18.
- [39] K. Leschonski, W. Alex, B. Koglin, *Teilchengrößenanalyse. 6. Trennverfahren (Fortsetzung)*, *Chem. Ing. Tech.* 45 (1974) 901–904.
- [40] J. Turkevich, P.C. Stevenson, J. Hillier, A study of the nucleation and growth processes in the synthesis of colloidal gold, *Discuss. Faraday Soc.* 11 (1951) 55.
- [41] J. Turkevich, P.C. Stevenson, J. Hillier, The formation of colloidal gold, *J. Phys. Chem.* 57 (1953) 670–673.
- [42] C. Metzger, A Novel Approach to Tailoring the Size of Quasi-Spherical Gold Nanoparticles, 2015.
- [43] N.G. Bastús, J. Comenge, V. Puntes, Kinetically controlled seeded growth synthesis of citrate-stabilized gold nanoparticles of up to 200 nm: size focusing versus Ostwald ripening, *Langmuir* 27 (2011) 11098–11105.
- [44] H. Herrmann, Zur Ermittlung der Trennkurve - Fehleranalyse und Fehlerverbesserung, *Chem. Ing. Tech.* 52 (1980) 466–467.
- [45] K. Leschonski, Das Klassieren disperster Feststoffe in gasförmigen Medien, *Chem. Ing. Tech.* 49 (1977) 708–719.